

## Observed El Niño SSTA Development and the Effects of Easterly and Westerly Wind Events in 2014/15

ANDREW M. CHIODI AND D. E. HARRISON

*Joint Institute for the Study of the Ocean and Atmosphere, University of Washington, and NOAA/Pacific Marine Environmental Laboratory, Seattle, Washington*

(Manuscript received 13 May 2016, in final form 10 November 2016)

### ABSTRACT


The unexpected halt of warm sea surface temperature anomaly (SSTA) growth in 2014 and development of a major El Niño in 2015 has drawn attention to our ability to understand and predict El Niño development. Wind stress–forced ocean model studies have satisfactorily reproduced observed equatorial Pacific SSTAs during periods when data return from the TAO/TRITON buoy network was high. Unfortunately, TAO/TRITON data return in 2014 was poor. To study 2014 SSTA development, the observed wind gaps must be filled. The hypothesis that subseasonal wind events provided the dominant driver of observed waveguide SSTA development in 2014 and 2015 is used along with the available buoy winds to construct an oceanic waveguide-wide surface stress field of westerly wind events (WWEs) and easterly wind surges (EWSs). It is found that the observed Niño-3.4 SSTA development in 2014 and 2015 can thereby be reproduced satisfactorily. Previous 2014 studies used other wind fields and reached differing conclusions about the importance of WWEs and EWSs. Experiment results herein help explain these inconsistencies, and clarify the relative importance of WWEs and EWSs. It is found that the springtime surplus of WWEs and summertime balance between WWEs and EWSs (yielding small net wind stress anomaly) accounts for the early development and midyear reversal of El Niño–like SSTA development in 2014. A strong abundance of WWEs in 2015 accounts for the rapid SSTA warming observed then. Accurately forecasting equatorial Pacific SSTA in years like 2014 and 2015 may require learning to predict WWE and EWS occurrence characteristics.

### 1. Introduction

The El Niño–Southern Oscillation (ENSO) phenomenon is Earth’s largest mode of coupled ocean–atmosphere variability that takes place on interannual time scales. ENSO’s warm (El Niño) and cool (La Niña) events are associated with major disruptions of the near-surface wind and upper ocean circulation across the tropical Pacific, which drive basin-scale changes in sea surface temperature anomalies (SSTAs) and can cause large-scale displacement of important Pacific fisheries. ENSO events are also associated with atmospheric circulation anomaly patterns that extend well outside of the tropical Pacific and influence seasonal weather conditions over land in many affected regions worldwide.

Skillful prediction of ENSO events provides a useful basis for seasonal weather forecasting where the weather associations are sufficiently strong in amplitude and consistent from event to event. Evidently, ENSO’s seasonal weather associations over land also drive substantial changes in the year-to-year variability of the global carbon cycle (Guerney et al. 2012; Chiodi and Harrison 2014). Yet, despite the improved understanding of coupled ocean–atmosphere physics earned by decades of study, accurately predicting the amplitudes and patterns of the SSTAs seen during ENSO events remains challenging.

The evolution of equatorial Pacific SSTA conditions during 2014 and 2015 offers an interesting opportunity to explore how well the observed SSTA can be understood based on our knowledge of the equatorial Pacific winds and their effects on the oceanic waveguide: Waveguide warming with a pattern typical for the early stages of El Niño events was observed in (boreal) spring of 2014, with the Niño-3.4 SSTA index reaching a value of  $+0.5^{\circ}\text{C}$  in May 2014. Widespread predictions for the continued development of an El Niño event followed

 Denotes content that is immediately available upon publication as open access.

Corresponding author e-mail: Andrew Chiodi, andy.chiodi@noaa.gov

the observed 2014 springtime warming, but the forecasted SSTA warming did not occur as predicted (McPhaden 2015). Instead, SSTAs in the central and eastern-central Pacific decreased during the summer, bringing ENSO SSTA conditions back to neutral (Niño-3.4 near 0°C) by the end of July 2014. More waveguide warming was observed in the fall of 2014 but the amplitudes were too weak for 2014 to decisively reach El Niño status by the end of the calendar year, when ENSO events are typically at their peak. Then, in the spring of 2015, warming with pattern similar to that of spring 2014—albeit stronger amplitude—was observed, followed by even stronger warming in the summer of 2015 that pushed the Niño-3.4 SSTA to  $>2.0^{\circ}\text{C}$  by the end of August 2015. The 2015 El Niño event stands, in terms of ENSO SSTA, as one of the larger observed in recent decades. What caused the 2014 El Niño development to stall in summer, and why was the summertime development in 2015 so different?

Menkes et al. (2014) attributed the observed springtime 2014 warming to a series of synoptic-scale westerly wind events (WWEs; also known as westerly wind bursts) based on the finding that their ocean general circulation model (OGCM) was able to accurately simulate the observed warming only when this series of WWEs was included in the applied forcing. Several recent studies have offered explanations for why the 2014 El Niño development stalled after this time, but their answers differ; some studies (Chen et al. 2015; Li et al. 2015; Menkes et al. 2014) have suggested that the distribution of westerly wind anomalies in 2014, including a lack of them in summer, is responsible for both the observed springtime increases and summertime decreases in ENSO SSTA. Others have suggested that easterly wind events, possibly with origin outside of the tropics (Zhu et al. 2016), are responsible; notably, Hu and Fedorov (2016), using a multisatellite-based wind product (NOAA Blended Sea Winds; Zhang et al. 2006), found a historically strong easterly wind event in June of 2014 and suggested that this easterly wind surge (EWS) was “the key dynamical factor that stalled [the 2014] El Niño development” (p. 2005). Min et al. (2015) reached a similar conclusion about the importance of the June 2014 EWS based on examination of wind estimates from the ERA-Interim, as well as the Japanese 55-year Reanalysis (JRA-55). The role of this EWS in limiting El Niño development in 2014 was also considered in the context of a conceptual ENSO model by Levine and McPhaden (2016). It bears noting here that the sources of wind information used by the studies that have rationalized the SSTA behavior observed in 2014 based mainly on the WWE distribution [all three used NCEP-1 or NCEP-2 reanalysis data; Chen et al. (2015)

also examined Tropical Atmosphere Ocean (TAO)/Triangle Trans-Ocean Buoy Network (TRITON) observations] are different from those that have focused instead on the waveguide cooling effects of EWSs.

Recently, we have revisited the question of how well the observed equatorial Pacific ENSO SSTA development can be simulated in an OGCM forced by surface wind stress (Chiodi and Harrison 2017). We did this over the first 20 years for which (nearly) complete TAO/TRITON buoy wind observations are available (1992–2011) using two types of wind information: 1) a field synthesized from the available buoy observations alone and 2) several widely used numerical weather prediction model reanalysis datasets, including NCEP-1, NCEP-2, and ERA-Interim. We found that: (i) there are oceanically important biases in the reanalysis wind data over the equatorial Pacific that often limit their usefulness for understanding the observed SSTA variability, and (ii) forcing the OGCM with TAO/TRITON winds can reproduce the major elements of SSTA variability during ENSO events with a (more) useful degree of accuracy (e.g., fall-average model–observation Niño-3.4 correlation of 0.93 and RMSE of  $0.49^{\circ}\text{C}$ ).

Here, we examine how well the observed rise and fall of El Niño-like SSTAs from spring to summer 2014, as well as the rapid El Niño development observed in 2015, can be understood in terms of our knowledge of the equatorial Pacific winds and their effects on the upper ocean. We again use the ocean model of Chiodi and Harrison (2017) and TAO/TRITON moored buoy wind observations to do this. Unfortunately, our knowledge of the winds during most of 2014 is more uncertain than is typical for the near 20 years over which the TAO/TRITON array has been fully deployed, due to the collapse of the array during 2012–14 (e.g., wind observations are available from the equatorial buoy line during 76% of the total possible buoy-days in the 1992–2011 period, but only 41% of the possible buoy-days in January–August 2014). In years with nearly full TAO/TRITON coverage, the gaps that occur when a few buoys fall out of service do not typically prevent the array from providing elementally accurate knowledge of the waveguide-wide wind field. This is because the wind conditions in a gap caused by the loss of a single buoy can still often be usefully estimated when bracketed by adjacent buoy wind observations (Harrison 1989; Chiodi and Harrison 2017). The unusually large extent of the gaps in 2014, however, extends beyond this feature of the array design.

We hypothesize that the wind events that occurred in 2014 and spring–summer 2015 are responsible for the observed ENSO SSTA development, and that the composite average wind event structure (based on previously observed wind events) provides a useful

TABLE 1. Day, center longitude, and amplitude scale factor of the WWEs and EWSs comprising the WE-constructed wind stress anomaly fields for 2014 and January through August of 2015.

Day of year	Center longitude (°E)	Amplitude scale factor	Type
2014			
2	220	0.8	EWS
10	185	0.6	EWS
24	149	1.0	WWE
56	160	0.9	WWE
76	180	0.7	WWE
107	165	0.6	WWE
154	188	0.5	EWS
175	165	0.35	WWE
185	178	0.5	EWS
203	150	0.7	WWE
215	190	0.9	WWE
215	230	0.4	WWE
247	190	0.7	WWE
271	147	0.5	WWE
287	190	0.6	WWE
307	210	0.5	WWE
348	195	0.6	WWE
350	240	0.5	WWE
2015			
5	260	0.3	EWS
8	155	0.9	WWE
20	195	0.9	WWE
38	160	1.2	WWE
67	240	0.4	EWS
76	160	1.3	WWE
78	255	0.6	WWE
86	190	0.8	WWE
125	160	1.5	WWE
133	225	0.7	WWE
149	192	0.6	WWE
155	260	0.4	WWE
165	195	0.2	EWS
178	160	1.3	WWE
188	190	0.4	WWE
192	225	0.9	WWE
200	195	0.3	WWE
215	165	1.3	WWE
232	215	1.0	WWE

template for estimating wind stress variability in the 2014 coverage gaps. Based on this hypothesis, we construct a wind stress field using equatorially centered WWE and EWS wind stress composites, which are fitted such that the constructed field is consistent with all available buoy wind observations. This strongly (but not rigorously, due to coverage gaps) constrains the  $x$  location, timing, and amplitudes of the fitted WWEs and EWSs, as is described in more detail in [section 3](#). Specification of these wind event occurrence statistics (as listed in [Table 1](#)), along with the WWE and EWS composites shown in [Fig. 1](#), define our hypothesized wind field. We use this WWE-/EWS-constructed wind stress field in two ways: on its own to force the OGCM,

and in combination with the available buoy wind observations to fill in the buoy coverage gaps. It will be shown that these two wind stress fields force nearly identical OGCM results, confirming that the wind event field is consistent with the observations from a forced ocean perspective. The high level of accuracy seen in the OGCM simulations forced by the resulting wind stress fields (as described in [section 5](#)) supports consideration of the hypothesized wind event scenario.

The synthesis of 2014 and 2015 (spring–summer) equatorial Pacific wind stress anomaly in terms of WWEs and EWSs permits an understanding of the observed Niño-3.4 behavior in terms of the effects of the wind events. We offer some experiments in which the

## Composite Subseasonal Wind Event Zonal Wind Stresss Anomalies

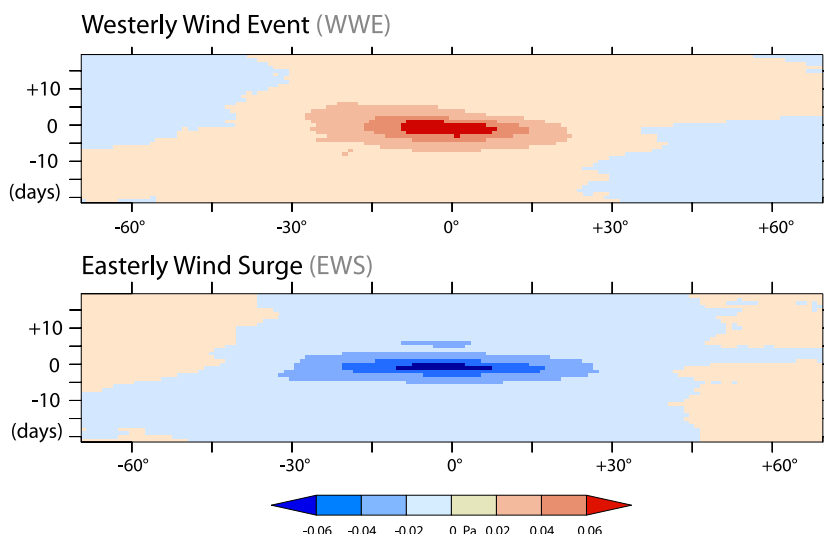


FIG. 1. (top) WWE and (bottom) EWS composite average wind stress anomalies.

seasonal distribution of wind events are juxtaposed between 2014 and 2015 to better understand why, in terms of the forced-ocean response to the respective wind event distributions, the springtime 2014 El Niño-like SSTA development was completely stalled by June ( $\sim 0^{\circ}\text{C}$  Niño-3.4) whereas the summer of 2015 exhibited rapid and consistent increases in ENSO SSTA. Since review of the previous 2014 studies motivates questions about the role of the June 2014 EWSs, we also offer results from an experiment that isolates their effects on 2014 SSTA development.

In separate experiments, we also force the model with zonal wind stress datasets used in the previously published 2014 case studies (NCEP-1, NCEP-2, ERA-Interim, and NOAA Blended Sea Winds) in order to better understand why different previous conclusions about the relative importance of WWEs and EWSs have been reached. Substantial differences are seen between the 2014 model results forced by these other wind stress products and those produced by the buoy wind observations and WWE and EWS construction. It is shown that the previous studies that have highlighted the role of EWSs in stalling the development of waveguide warming in 2014 are based on wind products with substantial easterly biases in them in 2014.

## 2. Data and methods

For SST information we use the NOAA Optimum Interpolation SST product, version 2 (NOAA OISST 2002), described by Reynolds et al. (2002) and provided by the NOAA/Oceanic and Atmospheric Research/Earth

System Research Laboratory Physical Sciences Division (Boulder, Colorado). As is the case for all variables used here, anomalies are calculated based on linear interpolation of the monthly mean climatology, base period 1986–2014.

We use daily average wind observations from the TAO/TRITON (TAO/TRITON 2000) moored buoy array described by McPhaden et al. (2010), and made available by the NOAA/Pacific Marine Environmental Laboratory TAO project office, to estimate wind stress. The daily average wind data are converted to daily average zonal pseudostress using the following formula:

$$\tau_x = \rho_a C_d |\mathbf{U}| u,$$

with air density  $\rho_a$  assigned the value of  $1.25 \text{ kg m}^{-3}$ , and the drag coefficient  $C_d$  is  $1.3 \times 10^{-3}$ ;  $\mathbf{U}$  is the 10-m wind vector and  $u$  its zonal component. This same formula for TAO-based pseudostress was also used by Harrison and Chiodi (2009), Hu and Fedorov (2016), and Chiodi and Harrison (2017).

We also use surface wind stress estimates from three numerical weather models run in data assimilation mode. These are the NCEP–NCAR Reanalysis-1 (NCEP1 1996) described by Kalnay et al. (1996), the NCEP–DOE Reanalysis-2 (NCEP2 2002), and the ERA-Interim (ERA-I 2011) described by Dee et al. (2011). These reanalysis products have also been used in the recent studies that examine 2014 equatorial Pacific SSTA development, as described in the introduction. In the NCEP-1 and NCEP-2 cases, daily average wind stress downloaded from the respective websites was used. In the

ERA-Interim case, daily averages were calculated based on the available 3-h averages. Wind stress from the NOAA Blended Sea Winds (NBSW) dataset (NBSW 2006), described by Zhang et al. (2006), is also used. This product relies on NCEP-2 for wind direction information and uses a blend of wind speed estimates from various satellite missions to estimate both the components of wind and wind stress. Herein, we use the NBSW-estimated wind information as well as the pseudostress formula listed above to estimate NBSW wind stress, as was also done by Hu and Fedorov (2016).

The OGCM we use is based on NOAA's Geophysical Fluid Dynamics Laboratory (GFDL) Modular Ocean Model, version 4 (MOM4; Griffies et al. 2003), employed here with the surface solar heat flux parameterization described by Harrison (1991). This model has been shown to reproduce climatological equatorial zonal currents and thermocline variability, as well as ENSO thermocline variability and aspects of equatorial upper ocean salinity variability in some previous experiments, when appropriately forced (Harrison et al. 1989, 1990, 2009; Harrison and Craig 1993; Chang et al. 2007). Our experimental procedure is similar to that of Harrison and Chiodi (2009), and was used more recently by Chiodi et al. (2014) and Chiodi and Harrison (2015, 2017). The model is first spun up by applying, over 30 years, the climatological wind stress and surface heat flux parameterization of Harrison et al. (2009). Then, in the experiment mode, the longwave and shortwave fluxes (based on model SSTs and specified constants; see Harrison 1991; Harrison et al. 2009) are specified as in the spinup, but sensible and latent heat fluxes are determined differently, according to the Philander and Siegel (1985) scheme, based on wind speed and a constant sea surface to near-surface differential in temperature ( $1^{\circ}\text{C}$ ) and near-surface relative humidity (0.8). Thus, the model SSTA development is not constrained in the experiment mode by any observed maritime temperature or humidity conditions. SSTAs are calculated based on the difference between control runs forced with climatological wind stress and experiment runs, in which zonal wind stress and the associated wind speed anomalies are also applied. In this configuration, changes in the winds affect both the applied momentum and turbulent surface heat fluxes, although experiments that omit the wind speed anomaly effects on turbulent surface heat flux reveal that momentum flux is the dominant driver of equatorial Pacific ENSO SSTA development in events like those considered herein (Chiodi and Harrison, 2017).

### 3. Synthesizing wind stress from TAO/TRITON wind observations

A key element of the TAO/TRITON array design is that the buoy spacing roughly matches the coherence

length scales of the observed winds in both the meridional ( $2^{\circ}$ – $3^{\circ}$ ) and zonal ( $\sim 15^{\circ}$ ) directions for all energetic periods greater than two days (Harrison and Luther 1990). This has motivated our initial approach to synthesizing a wind stress field from TAO/TRITON observations [also mentioned in Chiodi and Harrison (2017)], which we refer to as “TAO box” hereafter. In this case, boxes are drawn equidistant between the nominal buoy locations and filled with the respective TAO/TRITON pseudostress anomaly estimates, when available. The zonal spacing of these boxes is evident in Fig. 1, which shows the zonal pseudostress anomalies available, in a  $y$ -average sense, over the waveguide ( $2^{\circ}\text{S}$ – $2^{\circ}\text{N}$ ) in 2014.

To test our hypothesis that the observed SSTA development can be largely understood in terms of the effects of the westerly and easterly wind events that occur over the waveguide, we construct a wind stress anomaly field based on the linear superposition of equatorially centered wind events, with the wind event amplitudes, timing, and  $x$ -axis locations (longitudes) strongly constrained, although not rigorously defined by the available TAO/TRITON observations (Fig. 2); a more rigorous identification of wind events than is attempted here is made difficult due to the large number of TAO/TRITON gaps present in 2014. In many previous studies (including ours), wind events have been identified using reanalysis data, but in this case the apparent biases in the reanalysis products discussed below (cf. Chiodi and Harrison 2015, 2017) advise against doing that. To construct a representative wind event scenario based on the buoy observations, we first identified the times in which the daily-averaged TAO/TRITON observations reveal wind stress amplitudes greater than  $0.045\text{ Pa}$ , which is the wind event amplitude criterion used in Chiodi and Harrison (2015). This reveals localized instances of EWS-type behavior (i.e., patches of above-threshold easterlies, which, in this case, are often adjacent to coverage gaps) that occurred in January, June, and December of 2014. As is characteristic of EWSs, these easterly anomalies are mainly seen over the central to eastern central Pacific, and are highlighted in Fig. 2c by circumscribing blue lines. A larger amount of WWE-type behavior is also evident over the far western Pacific during each season. The observed westerly anomalies include a series of well-above-threshold ones during the beginning of the year [i.e., January–April (JFMA)], along with a patch of weaker amplitude, though still above threshold, anomalies in June, as well as another series of WWEs in the second half of the year (Fig. 2). We represent the observed behavior in terms of wind events by applying 12 WWEs and 4 EWS wind stress composites (Fig. 1) with  $x$  locations and timing set such that the applied WWE and EWS anomalies overlay

# TAO/Triton observed zonal wind stress anomaly

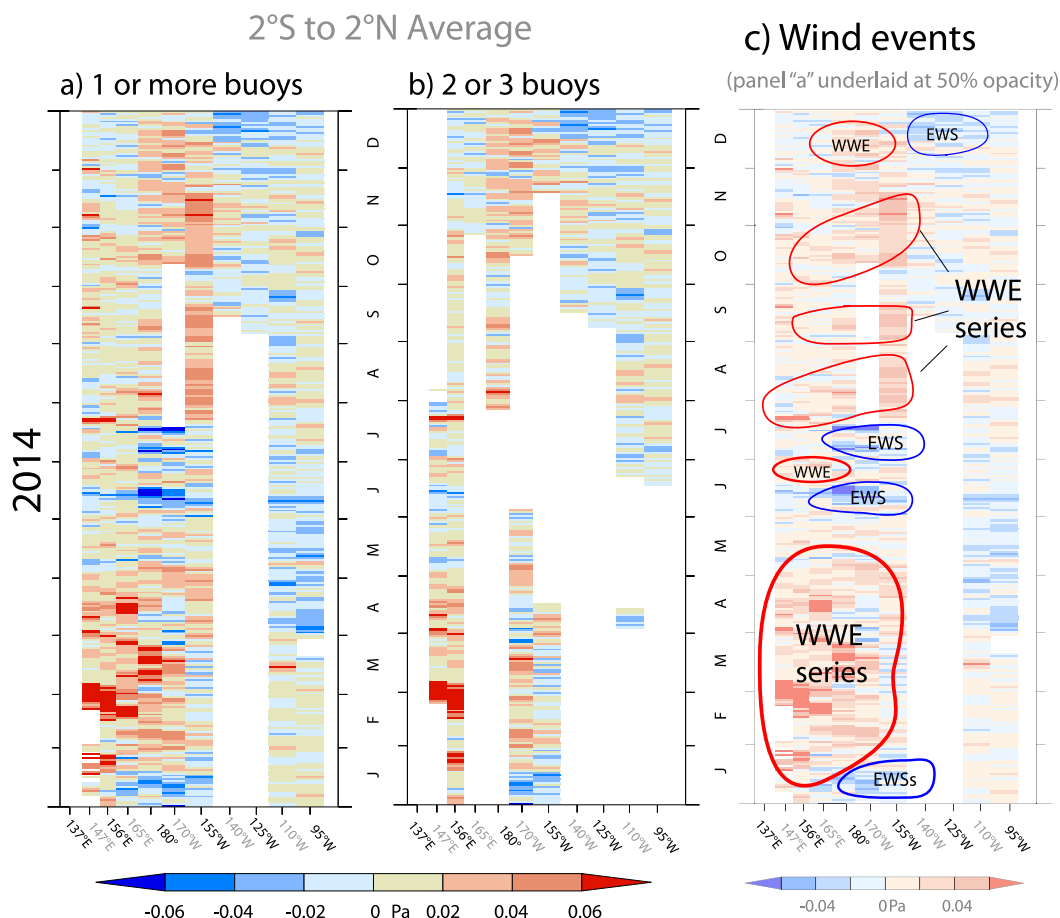


FIG. 2. TAO/TRITON-based wind stress anomalies in the core of the waveguide. (a) Averages of all available buoys from 2°S to 2°N, with blank space where no wind observations were made. (b) As in (a), but with anomalies shown only when at least 2 out of 3 buoys are available. (c) As in (a), but redrawn (fainter) with wind event activity circumscribed.

with the observed occurrences of event-like behavior. The amplitudes of the applied wind event composites in this case are multiplied by a scale factor (as listed in Table 1) approximated based on the number and strength of associated event-like wind observations (e.g., larger composite amplitudes are used to represent stronger amplitude and larger area patches of observed WWE-/EWS-type activity). The resulting wind stress anomaly field, referred to hereafter as the wind event (WE) construction, is shown in Fig. 3a.

We also synthesize another wind stress field by applying the TAO-box wind stress anomalies when observations are available, and filling gaps with the WE construction. We refer to this as the TAO-WE-filled wind stress field hereafter. As will be shown in the following section, the pure wind event scenario suggested here is sufficiently consistent with the available observations that

the WE-constructed and TAO-WE-filled wind stress anomaly fields drive very similar equatorial Pacific SSTA development in the ocean model (cf. Figs. 3a,b).

## 4. Simulating ENSO SSTA with easterly and westerly wind events

The WE-constructed 2014 equatorial Pacific wind stress field is shown again in Fig. 4 (left) alongside the SSTA produced when the WE construction is used to force the OGCM (left-center panel). The observed SSTA development pattern as well as its average over the Niño-3.4 region is also shown in Fig. 4 (right-center and right panels, respectively). The model simulation is successful in reproducing qualitatively correct equatorial SSTA pattern development, as well as an accurate Niño-3.4 trajectory (RMSE = 0.17°C). This suggests



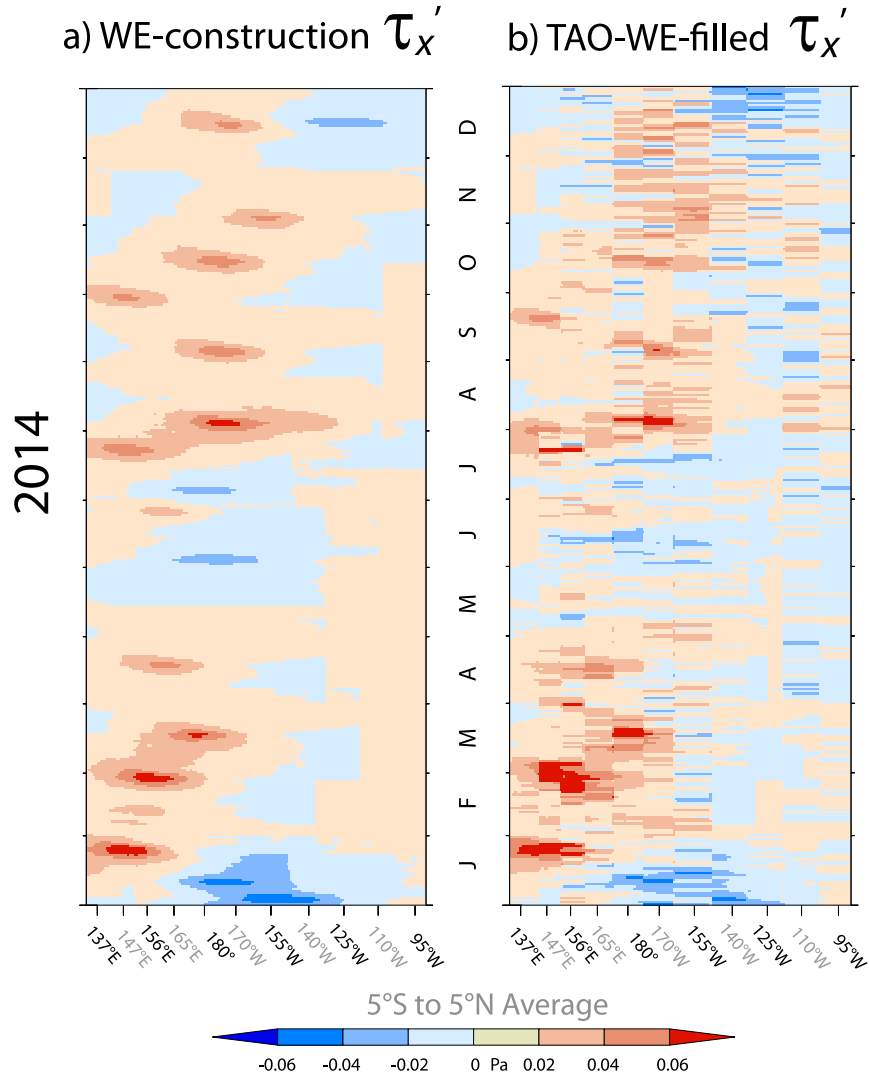


FIG. 3. 2014 (a) WWE- and EWS- (WE) constructed equatorial Pacific wind stress anomaly and (b) the wind stress field that results from substituting the available observations back into the WE-construction case (TAO-WE-filled wind stress anomaly).

that it is the character and distribution of wind events that is primarily responsible for the observed 2014 SSTA development.

Previous work has shown that anomalous surface advection by the wind-forced currents is the primary mechanism by which equatorial SSTA changes when forced by wind events during the onset and mature phases of El Niño and La Niña events (e.g., Chiodi and Harrison 2015). We have confirmed that this is also the case here.

Forcing the model with the 2014 WE-constructed and combined TAO-WE-filled wind stresses reproduces very similar patterns and amplitudes of ENSO SSTA development (Fig. 5), confirming that the WE construction has been constrained sufficiently by the

available buoy observations that the two wind stress fields are nearly identical in terms of their ability to drive satisfactorily accurate ENSO SSTA development in the ocean model.

It bears noting that accurate SSTA development is forced here with a wind stress field in which the late spring–early summertime wind events nearly cancel each other out in terms of net seasonal momentum flux [e.g., averaged zonally over the full basin and from 5°S to 5°N, the WE-constructed wind stress anomaly average for May–July ( $4 \times 10^{-4}$  Pa) is only about 5% of that seen over the earlier February–April period ( $7.1 \times 10^{-3}$  Pa)]. This near-tie between WWEs and EWSs in early summer has informed the experiment design described in section 5.

# 2014 Hindcast (WE-construction forced)

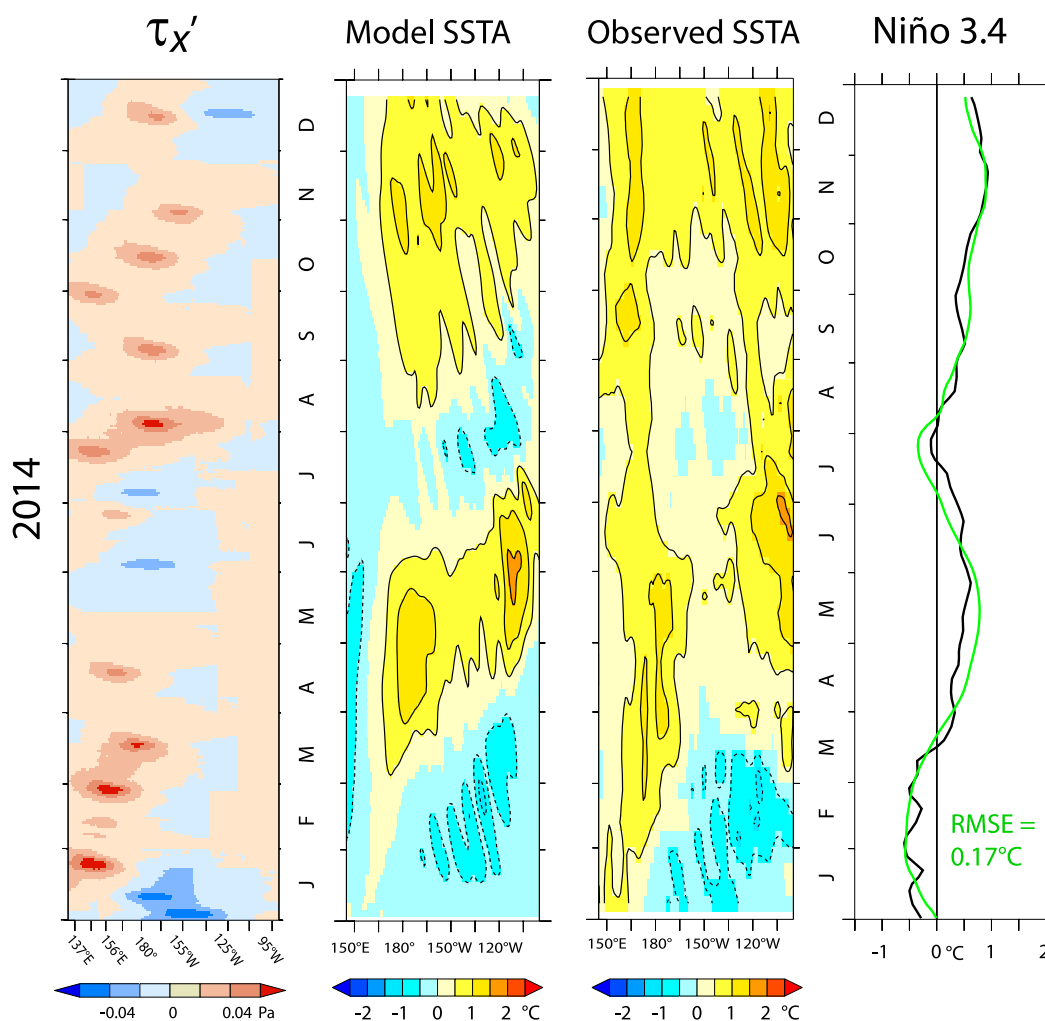


FIG. 4. (left)–(right) WE-constructed wind stress anomaly, and resulting OGCM equatorial SSTA, along with the observed SSTA, and modeled (green line) and observed (black line) Niño-3.4.

We have also constructed, by applying WWEs and EWSs, a wind stress field for spring and summer of 2015. Like its 2014 counterpart, the 2015 WE construction is sufficiently constrained by the available TAO/TRITON wind observations that the 2015 TAO-WE-filled and 2015 WE-constructed wind stresses drive nearly identical SSTA development in the OGCM. To accurately simulate 2015s SSTA development, the OGCM was started with initial oceanic conditions taken from the end of the 2014 WE-construction integration.

The fact that the observed 2015 spring–summer Niño-3.4 development is accurately reproduced in the OGCM in both cases (WE construction and TAO-WE-filled) suggests that wind events were a dominant driver of equatorial Pacific SSTA development in 2015. This also

permits an understanding of that development in terms of the applied wind event distribution characteristics.

## 5. Model experiments

We describe here results from a set of five experiments designed to highlight the wind event distribution differences that are responsible for the observed ENSO SSTA development differences between 2014 and 2015. These experiments are integrated over the eight calendar months of January through August. In the first and second experiments (Exps. 1 and 2) the wind events seen in the first four months of 2014 are applied to the model over the JFMA period, starting from the model's climatological initial ocean conditions. The next four months [May–August (MJJA)] are



## 2014 Hindcast (TAO-WE-filled)

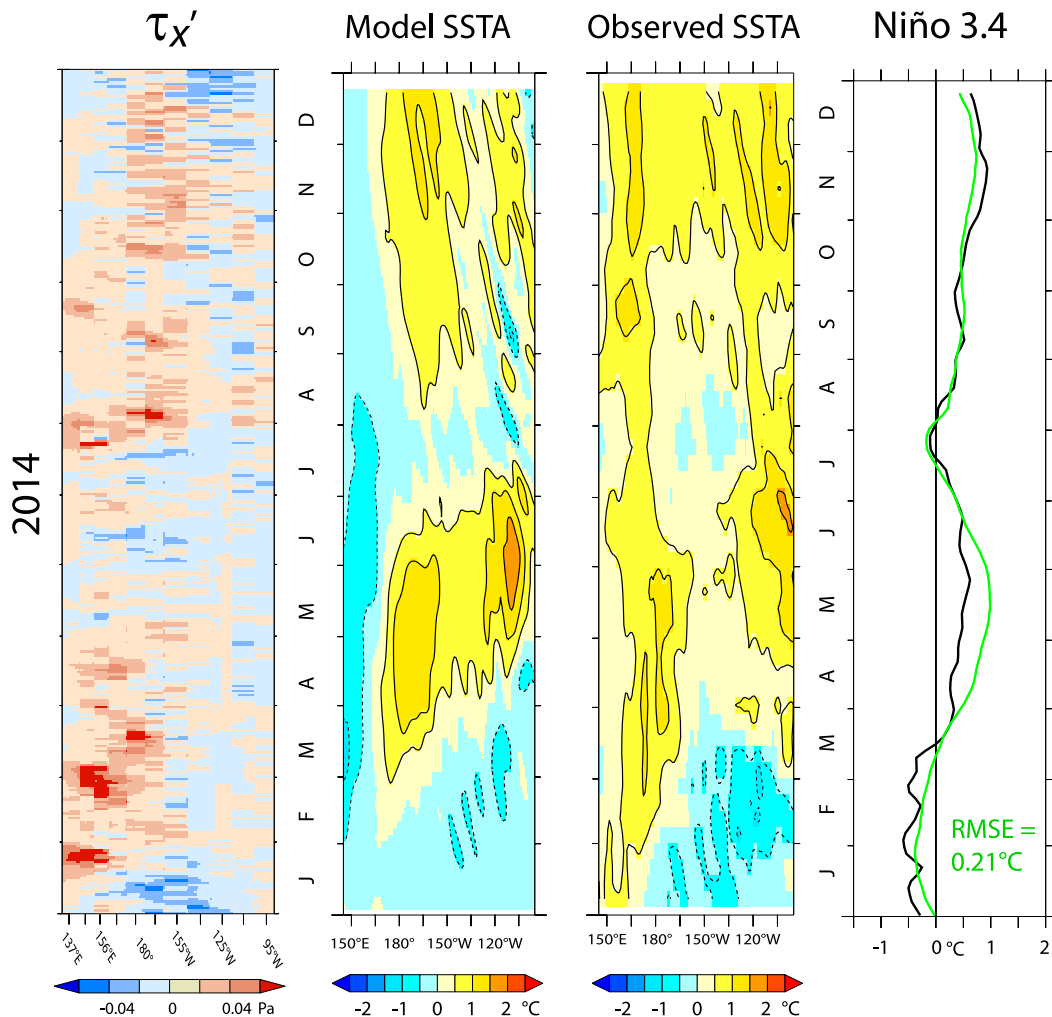


FIG. 5. As in Fig. 4, but with observed wind stresses substituted into the applied stress anomaly (TAO-WE-filled), when and where they are available.

forced differently: in Exp. 1 zero wind stress anomaly (i.e., climatological wind stress) is applied over MJJA, and in Exp. 2 the 2015 MJJA wind event distribution is instead applied over this time. The third and fourth experiments (Exps. 3 and 4) are forced with the 2015 JFMA wind event distribution over the first four months, starting from oceanic initial conditions taken from the end of our 2014 WE-construction run (Fig. 4). Then Exp. 3 is forced with the 2014 MJJA wind event distribution, and Exp. 4 is forced with zero wind stress anomaly over MJJA. In Exp. 5, the EWSs observed in June 2014 are removed from the 2014 WE-constructed wind stress field, and the resulting “no-June EWS” field is used to force the OGCM. Table 2 summarizes the initial oceanic conditions and wind stress anomaly forcing of these five experiments.

Experiment 1 results show that even with no wind stress anomaly applied after April, the model SSTAs rather accurately track the observed summertime Niño-3.4 decrease, reaching 0°C at the correct time of year (Fig. 6). This implies that an excess of easterly wind stress over summer is unnecessary for the springtime El Niño development to reverse course midyear. This result also demonstrates that the warming driven by a buildup of WWEs (as seen in spring 2014) should be expected to quickly cool if not sustained by subsequent westerly wind anomalies.

Results from Exp. 2 show that when the 2015 MJJA wind event distribution is instead applied following the 2014 spring, the model rapidly warms in summer, such that a Niño-3.4 trajectory like that observed in summer of 2015 is simulated (Fig. 6). This strongly suggests that the 2015

TABLE 2. Summary of the initial oceanic conditions and surface wind stress forcing used in the five experiments presented.

Expt	Initial ocean conditions	Wind stress anomaly forcing	
		JFMA	MJJA
1	Climatological	2014 WE-constructed	Zero
2	Climatological	2014 WE-constructed	2015 WE-constructed
3	2014 hindcast	2015 WE-constructed	2014 WE-constructed
4	2014 hindcast	2015 WE-constructed	Zero
5	Climatological	2014 WE-constructed	2014 no-June EWSs

summertime wind event distribution characteristics provided a dominant control on the observed end-of-summer 2015 Niño-3.4 value. Results from Exps. 3 and 4 (Fig. 7) also support this conclusion: in these cases, the well-simulated 2015 springtime warming quickly reverses course when it is not maintained by the 2015 summertime WWEs.

That the summertime Niño-3.4 cooling is more rapid and more strongly overshoots the 0°C level in Exp. 4 than in Exp. 1 suggests that ocean dynamics play a role in this cooling. We have confirmed that westward near-surface (5 m) ocean current anomalies develop over the Niño-3.4 region during June and July in Exps. 1 and 4 (even though zero wind stress anomaly is applied then), and that Exp. 4's westward anomalies are about 75% stronger than Exp. 1's in terms of the monthly-averaged peak over the Niño-3.4 region. Anomalous westward advection of the mean zonal SST gradient causes a surface cooling tendency over the central equatorial Pacific, where the mean

gradient is negative (cold tongue to the east and warm pool to the west). Min et al. (2015) found this term to be important over the central equatorial Pacific in summer 2014 based on their analysis of NCEP Global Ocean Data Assimilation (GODAS) data. Unfortunately, there are no TAO/TRITON ocean current observations available for data assimilation over the Niño-3.4 region in June–July of 2014 by which the zonal currents and associated temperature-gradient advection in the model/assimilation can be directly verified. What is nonetheless revealed by Exps. 1 and 4 is that direct wind stress forcing is not necessary for such anomalous zonal advection to occur.

When, instead of zero anomaly, the 2014 MJJA wind event distribution is applied following the 2015 JFMA events (Exp. 3; Fig. 7), a Niño-3.4 trajectory qualitatively similar to that in Exp. 4 is produced, except in this case the overshoot into negative Niño-3.4 is somewhat more rapid and stronger since it is aided by the pair of

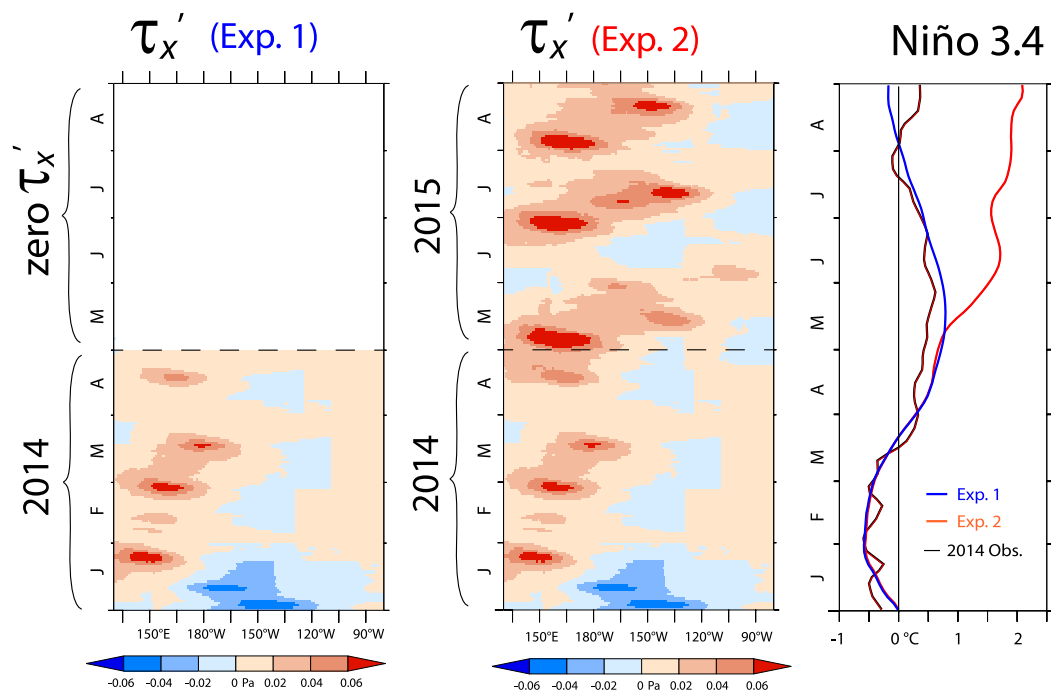


FIG. 6. Wind stress anomaly forcing and simulated Niño-3.4 response from Exps. 1 and 2.

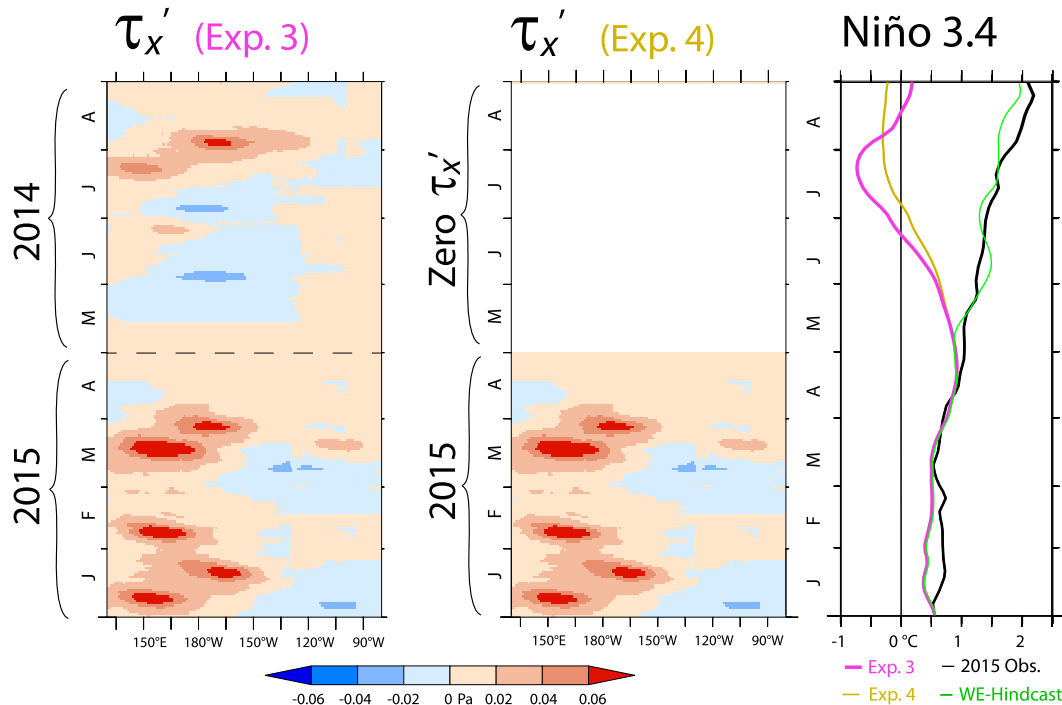


FIG. 7. Wind stress anomaly forcing and simulated Niño-3.4 response from Exps. 3 and 4. Shown also is the Niño-3.4 response in the 2015 WE-construction hindcast (green line).

June EWSs. A second warming tendency is then driven by the WWEs that occur near the end of summer 2014.

The SSTA tendency driven by the June EWSs is illustrated in Fig. 8, which shows results from Exp. 5 and the 2014 WE-construction hindcast. These two runs differ only in that the June EWSs were removed from the wind stress forcing in Exp. 5. Comparison of the run with and without the June EWSs reveals that they drive approximately  $0.4^{\circ}\text{C}$  cooling averaged over the Niño-3.4 region and mid-June through August, with a weekly-averaged peak difference of approximately  $0.6^{\circ}\text{C}$  at the end of July. Even with these EWSs removed, Niño-3.4 cooling is seen over the May–July period in Exp. 5 with amplitude comparable to that observed.

## 6. OGCM simulations using other wind stress datasets

We have also attempted to simulate 2014 equatorial Pacific SSTA using the OGCM and wind stress data provided by the reanalyses NCEP-1, NCEP-2, and ERA-Interim, as well as the satellite and NCEP-2–based NBSW product (Fig. 9). Of these four other simulations, it is the NCEP-1–forced simulation that simulates the Niño-3.4 trajectory with the lowest amount of error ( $\text{RMSE} = 0.35^{\circ}\text{C}$ ). This level of error, however, is still 94% (66%) larger than the WE-construction (TAO-WE-filled)

simulation described above. In the NCEP-1–forced OGCM simulation there is a warm bias of a few tenths of a degree Celsius that is apparent throughout most of the year, including summer, when it fails to cool all the way to  $0^{\circ}\text{C}$  as was observed. This suggests that the NCEP-1 product underrepresents the EWS activity that occurred in early and mid-2014. Nonetheless, the NCEP-1 simulation ends with a Niño-3.4 value close to that observed. The NCEP-2 simulation closely tracks NCEP-1 during the first half of the year but exhibits more summertime cooling than NCEP-1. The NCEP-2 case, however, stays cooler than the observed SSTAs in the fall, resulting in a somewhat higher RMSE of  $0.42^{\circ}\text{C}$ .

Larger errors are produced by forcing the OGCM with ERA-Interim and NBSW wind stress estimates. Although the springtime Niño-3.4 development produced in these two cases is basically similar to that observed, the simulated summertime cooling is much too strong, overshooting the observed minimum by approximately  $0.75^{\circ}$  and  $1.5^{\circ}\text{C}$ , respectively. Evidently, the amplitudes of the midyear easterly wind stress anomalies represented in these datasets are much too large. Our recent study of forced OGCM simulations over the 1992–2011 period (Chiodi and Harrison 2017) has revealed that ERA-Interim has had an oceanically important easterly bias in zonal wind stress relative to the TAO/TRITON observations in each year since 2004 (although it exhibited mainly westerly biases in the 1990s).

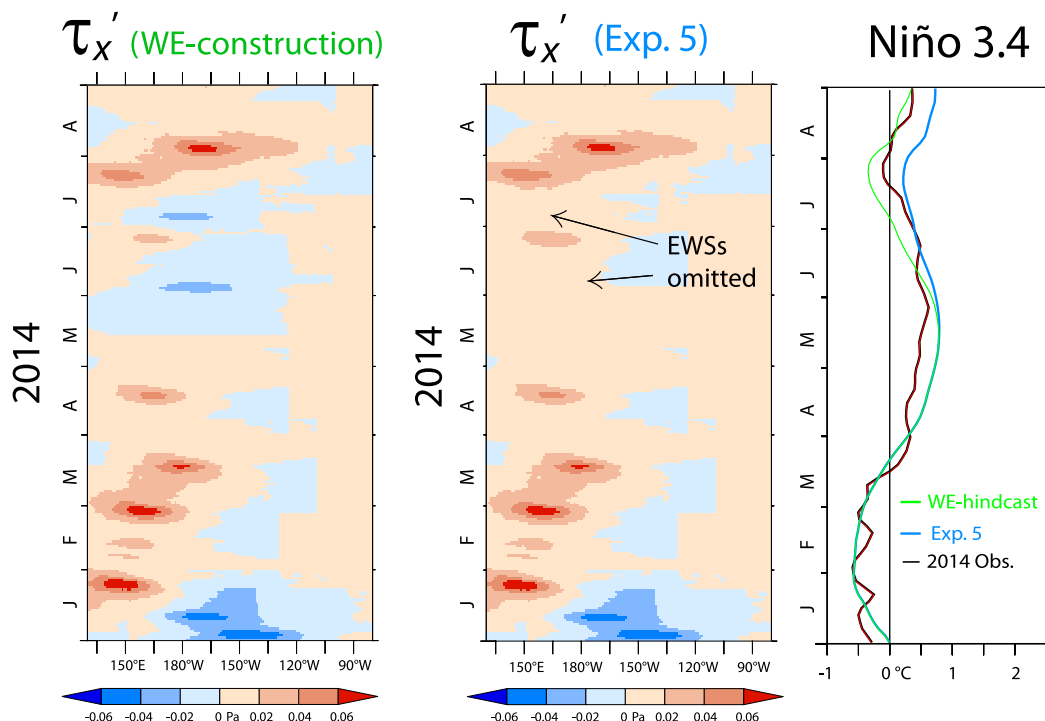


FIG. 8. Wind stress anomaly forcing and simulated Niño-3.4 response in 2014 hindcast (repeated here from Fig. 4 between January and August for comparison) and Exp. 5.

This result shows that the post-2004 tendency for easterly bias in ERA-Interim extends to 2014.

The NBSW product drives a cool bias in the OGCM that is twice as large as with ERA-Interim. This strongly suggests that the EWSs represented in NBSW are unrealistically large. Previous claims that these easterlies were historically large may deserve reconsideration.

Although it is missing about half of the wind observations that would have been made at full coverage, the TAO-box wind stress is still able to simulate the observed Niño-3.4 behavior with at least as much accuracy as any of the other datasets discussed above ( $\text{RMSE} = 0.32^\circ\text{C}$ ). In this case, observed Niño-3.4 SSTA is cooler than the simulation in the first two months of the year, and the late-year warming is stronger in the observations than the model. Notwithstanding these errors, a behavior qualitatively consistent with that observed is still forced in the OGCM in this case, supporting the view that the array design is capable of compensating for a few buoy dropouts and still being able to accurately measure the elemental wind stress variability associated with ENSO, but not as many as occurred in 2014.

## 7. Discussion and conclusions

We have shown that wind stress fields constructed by applying equatorially centered WWE and EWS composites are capable of accurately simulating the ENSO SSTA

development observed in 2014, as well as spring and summer of 2015. Rigorous WWE and EWS identification is made difficult in 2014 by the unusually sparse availability of TAO/TRITON winds then. The constructed fields are, nonetheless, strongly constrained by the available buoy wind observations, and very little changed in terms of their forced-ocean response when the available wind observations are substituted back into them. These results suggest that the distribution of wind events in each year played a dominant role in determining the respective equatorial Pacific SSTA development. These results also permit an understanding of SSTA development in terms of the effects of the wind event effects.

The 2014 wind event distribution, after some early (January) easterlies, exhibited a series of WWEs in spring, and then a mix of lower-amplitude WWEs along with a couple of EWSs in summer. Previous studies have reached different conclusions about the relative importance of the WWEs and EWSs in driving the observed 2014 ENSO SSTA development, which warmed in spring but cooled in summer. The experiment results discussed above do not support the previous claims that it took an especially strong EWS to cause the summertime SSTA cooling. The strongest such claims were based on the satellite-based NOAA Blended Sea Winds dataset, which, relative to the TAO/TRITON observations, exhibits an unrealistically strong easterly bias in the summer of 2014

## 2014 Niño 3.4 Hindcasts

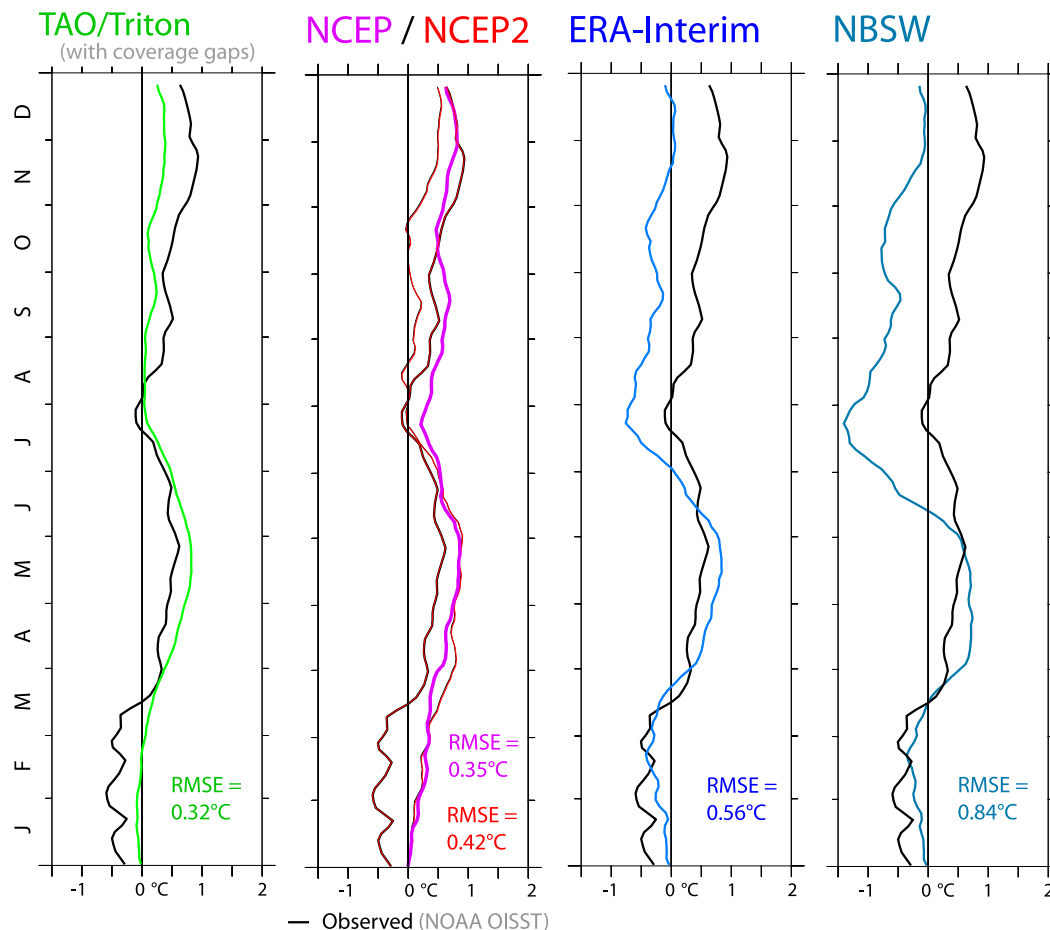


FIG. 9. OGCM-simulated 2014 Niño-3.4 forced by applying (left)–(right) the TAO box, NCEP-1 and NCEP-2, ERA-Interim, and NOAA Blended Sea Winds wind stress anomalies. The observed trajectory is drawn with the black line in each panel.

that forces our ocean model's midyear Niño-3.4 value to be much cooler than observed ( $\sim 1.5^{\circ}\text{C}$ ). This serves as a cautionary reminder that it is important to check wind products like this one against high-quality observations to understand the observed behavior of the coupled system.

Results show that after the 2014 springtime SSTA development is accurately forced in our OGCM by the early-year wind event distribution, the summertime decrease is also accurately simulated even when no further wind stress anomalies are applied. The notable characteristic of the mid-2014 wind event distribution in this context is that it resulted in neither a strong surplus of net westward nor eastward surface momentum flux. The model behavior seen during this time is consistent with the previous observational work of [Vecchi and Harrison \(2000\)](#), which showed that, on average, waveguide warming is observed following the WWEs that occur in ENSO-neutral

conditions, whereas once already warmed, the waveguide tends to cool if this warming is not maintained by a surplus of subsequent WWEs. The behavior observed during spring and summer of 2014 can now be understood as a case example of the SSTA changes previously observed following WWEs in a composite average sense.

As in 2014, 2015 began with a series of WWEs, except stronger. WWE wind stress anomalies equivalent to 3.2 and 5.7 WWE composites were applied to our OGCM to realistically simulate waveguide SSTA development over the first four months of 2014 and 2015, respectively. Subsequent experiments show that in both cases, the waveguide SSTA warming driven by the springtime WWEs quickly cools when it is not maintained by further WWE activity. An interesting point of comparison between the experiments in which wind stress anomalies were applied to the model only through April is that the

summertime cooling seen in the 2015 case is stronger than that seen in the 2014 case. This highlights the role of ocean dynamics in the post-WWE cooling. Equatorially trapped oceanic Rossby wave reflection off the western boundary has long been included in theories for year-to-year reversals in the state of the coupled tropical Pacific system (Schopf and Suarez 1988), but their role in shaping season-to-season changes has received less attention. Examination of the processes that cause warm (cool) ENSO SSTA development to quickly reverse course, if not maintained by westerly (easterly) wind anomalies, may provide useful grounds for future study.

In our model simulations, the primary reason why the summer of 2015 exhibited strong El Niño SSTA development and the summer of 2014 did not is that the summertime WWEs in 2015 were much stronger and more frequent than in 2014. During the summer of 2015, accurate Niño-3.4 behavior was simulated in our OGCM by applying the equivalent of 8.4 average-sized WWEs during MJJA, whereas accurate summertime 2014 behavior was forced by applying only 2.4 WWEs, along with a couple of moderate EWSs. Additional experiments revealed that the model is able to simulate 2015-like summertime Niño-3.4 development as long as it is forced with the 2015 summertime WWE distribution, regardless of which wind event distribution (2014 or 2015) was applied in the beginning of the year. This suggests that strong El Niño-like SSTA development will follow any equatorial wind event distribution that is as strongly skewed in favor of the WWEs as was the case in the summer–fall 2015.

Thus, the observed ENSO SSTA development in 2014 and 2015 is understandable from the forced-ocean perspective, based on the respective wind event distributions. But what caused the 2014 and 2015 wind event distributions to be so different? Comparison of the wind event behavior seen in these two years with what has been learned previously about the relationship between wind event frequency and ENSO SSTA conditions offers some useful insight, but also highlights an important open question. It is useful to recall that WWEs, based on the definition used here, have an average frequency that increases from about 1 to about 2 events month<sup>−1</sup> as the waveguide warms from ENSO-neutral to warm-ENSO SSTA conditions (Vecchi and Harrison 2000; cf. Gebbie et al. 2007). EWSs also have an average occurrence frequency of about 1 event month<sup>−1</sup> and may decrease in number as the system warms (c.f. Chiodi and Harrison 2015; Puy et al. 2016). These wind event occurrence statistics suggest a struggle in neutral conditions between the EWSs and WWEs for control of that year's ENSO SSTA trajectory. That the 2015 summertime WWE distribution exhibited roughly 2 WWEs month<sup>−1</sup> (~8 WWEs over four months, with little EWS activity) and occurred

during warm-ENSO SSTA conditions (May 2015 started with Niño-3.4 values around +1°C and August 2015 ended near +2°C) makes it remarkably consistent with the previously observed warm-ENSO-average frequency of approximately 2 WWEs month<sup>−1</sup>. It can also be said that the 2014 summertime wind event distribution is at least roughly consistent with the average ENSO-neutral wind event occurrence statistics in that no clear winner between the EWSs and WWEs emerged, and Niño-3.4 values were in the ENSO-neutral range then [April–August (January–August) averaged Niño-3.4 SSTA was only ~0.3°C (0.1°C)]. The years 2014 and 2012 before it (Su et al. 2014), which were predicted to develop into substantial El Niño events but did not, serve as a reminder that it remains difficult, starting from neutral conditions, to anticipate when one type of wind event will sufficiently dominate the distribution to drive and maintain ENSO SSTA development. It is also difficult to know if or when there is a point in that development at which sustained wind event dominance of one type or the other can be reliably expected to continue through the end of the calendar year. Improving our ability to predict these aspects of ENSO development may require learning to predict the distributions of easterly and westerly wind events in ENSO-neutral conditions. It is an open question whether there are factors that control, in a predictable way, the distribution of wind events in weak-ENSO anomaly states, or if their occurrence statistics will continue to appear, to our knowledge, to be essentially random.

**Acknowledgments.** This publication is partially funded by the Joint Institute for the Study of the Atmosphere and Ocean (JISAO) under NOAA Cooperative Agreement NA10OAR4320148, and by support from the Climate Observations Division of the NOAA Climate Program Office (FundRef 100007298) as well as from NOAA's Pacific Marine Environmental Laboratory.

## REFERENCES

- Chang, Y.-S., C.-W. Cho, Y.-H. Youn, and J.-W. Seo, 2007: Validation of ocean general circulation model (FMS-MOM4) in relation with climatological and Argo data. *J. Korean Earth Sci. Soc.*, **28**, 545–555, doi:10.5467/JKESS.2007.28.5.545.
- Chen, D., and Coauthors, 2015: Strong influence of westerly wind bursts on El Niño diversity. *Nat. Geosci.*, **8**, 339–345, doi:10.1038/ngeo2399.
- Chiodi, A. M., and D. E. Harrison, 2014: Comment on Qian et al. 2008: La Niña and El Niño composites of atmospheric CO<sub>2</sub> change. *Tellus*, **66B**, 20428, doi:10.3402/tellusb.v66.20428.
- , and —, 2015: Equatorial Pacific easterly wind surges and the onset of La Niña events. *J. Climate*, **28**, 776–792, doi:10.1175/JCLI-D-14-00227.1.
- , and —, 2017: Simulating ENSO SSTA from TAO/TRITON winds: The impacts of 20 years of buoy observations in the



- waveguide and comparison with reanalysis products. *J. Climate*, **30**, 1041–1059, doi:[10.1175/JCLI-D-15-0865.1](https://doi.org/10.1175/JCLI-D-15-0865.1).
- , —, and G. A. Vecchi, 2014: Subseasonal atmospheric variability and El Niño waveguide warming: Observed effects of the Madden-Julian oscillation and westerly wind events. *J. Climate*, **27**, 3619–3642, doi:[10.1175/JCLI-D-13-00547.1](https://doi.org/10.1175/JCLI-D-13-00547.1).
- Dee, D. P., and Coauthors, 2011: The ERA-Interim reanalysis: Configuration and performance of the data assimilation system. *Quart. J. Roy. Meteor. Soc.*, **137**, 553–597, doi:[10.1002/qj.828](https://doi.org/10.1002/qj.828).
- ERA-I, 2011: The ERA-Interim reanalysis. European Centre for Medium-Range Weather Forecasts (ECMWF). Accessed 15 February 2016. [Available online at <http://apps.ecmwf.int/datasets/data/interim-full-daily>.]
- Gebbie, G., I. Eisenman, A. Wittenberg, and E. Tziperman, 2007: Modulation of westerly wind bursts by sea surface temperature: A semistochastic feedback for ENSO. *J. Atmos. Sci.*, **64**, 3281–3295, doi:[10.1175/JAS4029.1](https://doi.org/10.1175/JAS4029.1).
- Griffies, S. M., M. J. Harrison, R. C. Pacanowski, and A. Rosati, 2003: A technical guide to MOM4. GFDL Ocean Group Tech. Rep. 5, NOAA/Geophysical Fluid Dynamics Laboratory, 295 pp.
- Guernsey, K. R., K. Castillo, B. Li, and Z. Zhang, 2012: A positive carbon feedback to ENSO and volcanic aerosols in the tropical terrestrial biosphere. *Global Biogeochem. Cycles*, **26**, GB1029, doi:[10.1029/2011GB004129](https://doi.org/10.1029/2011GB004129).
- Harrison, D. E., 1989: On climatological monthly mean wind stress and wind stress curl fields over the world ocean. *J. Climate*, **2**, 57–70, doi:[10.1175/1520-0442\(1989\)002<0057:OCMMWS>2.0.CO;2](https://doi.org/10.1175/1520-0442(1989)002<0057:OCMMWS>2.0.CO;2).
- , 1991: Equatorial sea surface temperature sensitivity to net surface heat flux: Some ocean circulation model results. *J. Climate*, **4**, 539–549, doi:[10.1175/1520-0442\(1991\)004<0539:ESSTST>2.0.CO;2](https://doi.org/10.1175/1520-0442(1991)004<0539:ESSTST>2.0.CO;2).
- , and D. S. Luther, 1990: Surface winds from tropical Pacific islands—Climatological statistics. *J. Climate*, **3**, 251–271, doi:[10.1175/1520-0442\(1990\)003<0251:SWFTPI>2.0.CO;2](https://doi.org/10.1175/1520-0442(1990)003<0251:SWFTPI>2.0.CO;2).
- , and A. P. Craig, 1993: Ocean model studies of upper-ocean variability at 0°, 160°W during the 1982–1983 ENSO: Local and remotely forced response. *J. Phys. Oceanogr.*, **23**, 425–451, doi:[10.1175/1520-0485\(1993\)023<0425:OMSOUO>2.0.CO;2](https://doi.org/10.1175/1520-0485(1993)023<0425:OMSOUO>2.0.CO;2).
- , and A. M. Chiodi, 2009: Pre- and post-1997/98 westerly wind events and equatorial Pacific cold tongue warming. *J. Climate*, **22**, 568–581, doi:[10.1175/2008JCLI2270.1](https://doi.org/10.1175/2008JCLI2270.1).
- , W. S. Kessler, and B. S. Giese, 1989: Ocean circulation model hindcasts of the 1982–83 El Niño: Thermal variability along the ship-of-opportunity tracks. *J. Phys. Oceanogr.*, **19**, 397–418, doi:[10.1175/1520-0485\(1989\)019<0397:OCMHOT>2.0.CO;2](https://doi.org/10.1175/1520-0485(1989)019<0397:OCMHOT>2.0.CO;2).
- , B. S. Giese, and E. S. Sarachik, 1990: Mechanisms of SST change in the equatorial waveguide during the 1982–83 ENSO. *J. Climate*, **3**, 173–188, doi:[10.1175/1520-0442\(1990\)003<0173:MOSCI>2.0.CO;2](https://doi.org/10.1175/1520-0442(1990)003<0173:MOSCI>2.0.CO;2).
- , A. Chiodi, and G. Vecchi, 2009: Effects of surface forcing on the seasonal cycle of the eastern equatorial Pacific. *J. Mar. Res.*, **67**, 701–729, doi:[10.1357/002224009792006179](https://doi.org/10.1357/002224009792006179).
- Hu, S., and A. V. Fedorov, 2016: Exceptionally strong easterly wind burst stalling El Niño of 2014. *Proc. Natl. Acad. Sci. USA*, **113**, 2005–2010, doi:[10.1073/pnas.1514182113](https://doi.org/10.1073/pnas.1514182113).
- Kalnay, E., and Coauthors, 1996: The NCEP/NCAR 40-Year Reanalysis Project. *Bull. Amer. Meteor. Soc.*, **77**, 437–471, doi:[10.1175/1520-0477\(1996\)077<0437:TNYRP>2.0.CO;2](https://doi.org/10.1175/1520-0477(1996)077<0437:TNYRP>2.0.CO;2).
- Levine, A. F. Z., and M. J. McPhaden, 2016: How the July 2014 easterly wind burst gave the 2015–2016 El Niño a head start. *Geophys. Res. Lett.*, **43**, 6503–6510, doi:[10.1002/2016GL069204](https://doi.org/10.1002/2016GL069204).
- Li, J., B. Liu, J. Li, and J. Mao, 2015: A comparative study on the dominant factors responsible for the weaker-than-expected El Niño event in 2014. *Adv. Atmos. Sci.*, **32**, 1381–1390, doi:[10.1007/s00376-015-4269-6](https://doi.org/10.1007/s00376-015-4269-6).
- McPhaden, M. J., 2015: Paying hide and seek with El Niño. *Nat. Climate Change*, **5**, 791–795, doi:[10.1038/nclimate2775](https://doi.org/10.1038/nclimate2775).
- , and Coauthors, 2010: The global tropical moored buoy array. *Proc. OceanObs'09: Sustained Ocean Observations and Information for Society Conf.*, Vol. 2, Venice, Italy, ESA Publication WPP-306. [Available online at [www.aoml.noaa.gov/phod/docs/McPhaden\\_TheGlobalTropical.pdf](http://www.aoml.noaa.gov/phod/docs/McPhaden_TheGlobalTropical.pdf).]
- Menkes, C. E., M. Lengaigne, J. Vialard, M. Puy, P. Marchesiello, S. Cravatte, and G. Cambon, 2014: About the role of Westerly Wind Events in the possible development of an El Niño in 2014. *Geophys. Res. Lett.*, **41**, 6476–6483, doi:[10.1002/2014GL061186](https://doi.org/10.1002/2014GL061186).
- Min, Q., J. Su, R. Zhang, and X. Rong, 2015: What hindered the El Niño pattern in 2014? *Geophys. Res. Lett.*, **42**, 6762–6770, doi:[10.1002/2015GL064899](https://doi.org/10.1002/2015GL064899).
- NBSW, 2006: NOAA Blended Sea Winds. NOAA/NESDIS/National Climatic Data Center. Accessed 9 March 2016. [Available online at <https://www.ncdc.noaa.gov/oa/rsad/air-sea/seawinds.html>.]
- NCEP1, 1996: NCEP/NCAR Reanalysis. NOAA/OAR/ESRL PSD. Accessed 15 September 2015. [Available online at <http://www.esrl.noaa.gov/psd/data/gridded/data.ncep.reanalysis.html>.]
- NCEP2, 2002: NCEP–DOE Reanalysis 2. NOAA/OAR/ESRL PSD. Accessed 1 March 2016. [Available online at <http://www.esrl.noaa.gov/psd/data/gridded/data.ncep.reanalysis2.html>.]
- NOAA OISST, 2002: NOAA Optimum Interpolation Sea Surface Temperature version 2. NOAA/OAR/ESRL PSD. Accessed 15 September 2015. [Available online at <http://www.esrl.noaa.gov/psd/data/gridded/data.noaa.oisst.v2.html>.]
- Philander, S. G. H., and A. D. Siegel, 1985: Simulation of El Niño of 1982–83. *Coupled Ocean–Atmosphere Models*, J. Nihoul, Ed., Elsevier, 517–541.
- Puy, M., J. Vialard, M. Lengaigne, and E. Guilyardi, 2016: Modulation of equatorial Pacific westerly/easterly wind events by the Madden-Julian oscillation and convectively-coupled Rossby waves. *Climate Dyn.*, **46**, 2155–2178, doi:[10.1007/s00382-015-2695-x](https://doi.org/10.1007/s00382-015-2695-x).
- Reynolds, R. W., N. A. Rayner, T. M. Smith, D. C. Stokes, and W. Wang, 2002: An improved in situ and satellite SST analysis for climate. *J. Climate*, **15**, 1609–1625, doi:[10.1175/1520-0442\(2002\)015<1609:AHSAS>2.0.CO;2](https://doi.org/10.1175/1520-0442(2002)015<1609:AHSAS>2.0.CO;2).
- Schopf, P. S., and M. J. Suarez, 1988: A delayed action oscillator for ENSO. *J. Atmos. Sci.*, **45**, 549–566, doi:[10.1175/1520-0469\(1988\)045<0549:VIACOM>2.0.CO;2](https://doi.org/10.1175/1520-0469(1988)045<0549:VIACOM>2.0.CO;2).
- Su, J., B. Xiang, B. Wang, and T. Li, 2014: Abrupt termination of the 2012 Pacific warming and its implication on ENSO prediction. *Geophys. Res. Lett.*, **41**, 9058–9064, doi:[10.1002/2014GL062380](https://doi.org/10.1002/2014GL062380).
- TAO/TRITON, 2000: Tropical Atmosphere Ocean/Triangle Trans-Ocean Buoy Network. NOAA/PMEL TAO project office. Accessed 15 September 2015. [Available online at [http://www.pmel.noaa.gov/tao/data\\_deliv/frames/main.html](http://www.pmel.noaa.gov/tao/data_deliv/frames/main.html).]
- Vecchi, G. A., and D. E. Harrison, 2000: Tropical Pacific sea surface temperature anomalies, El Niño, and equatorial westerly wind events. *J. Climate*, **13**, 1814–1830, doi:[10.1175/1520-0442\(2000\)013<1814:TPSSTA>2.0.CO;2](https://doi.org/10.1175/1520-0442(2000)013<1814:TPSSTA>2.0.CO;2).
- Zhang, H.-M., J. J. Bates, and R. W. Reynolds, 2006: Assessment of composite global sampling: Sea surface wind speed. *Geophys. Res. Lett.*, **33**, L17714, doi:[10.1029/2006GL027086](https://doi.org/10.1029/2006GL027086).
- Zhu, J., A. Kumar, B. Huang, M. A. Balmaseda, Z.-Z. Hu, L. Marx, and J. L. Kinter III, 2016: The role of off-equatorial surface temperature anomalies in the 2014 El Niño prediction. *Sci. Rep.*, **6**, 19677, doi:[10.1038/srep19677](https://doi.org/10.1038/srep19677).